Simple incremental approach for analysing optimal non-prismatic functionally graded beams

Hassina Ziou[1], and Mohamed Guenfoud [2]

[1] *National Centre for Studies and Integrated Research on Building (CNERIB), 16097, Souidania, Algiers, Algeria*

[2] *University of Guelma, faculty of science and technology, Department of Civil and Hydraulic Engineering, BP 401 Guelma 24000, Algeria*

Corresponding author:
Hassina Ziou
ziou.hassina@univ-guelma.dz

Abstract:
This paper presents a simple incremental approach of analysing the static behaviour of functionally graded tapered beams. This approach involves dividing the non-uniform beam into segments with uniform cross-sections, and using two separate finite element models to analyse the structural behavior of slender beams (Euler-Bernoulli model) and deep beams (Timoshenko beam theory). The material properties of the beam vary according to a power law distribution through the thickness, resulting in smooth variations in the mechanical properties. The finite element system of equations is obtained using the principle of virtual work. Detailed information on the shape functions and stiffness matrix of the beam is provided, and the numerical results are evaluated and validated using data from the literature. The comparison demonstrates that the response of the functionally graded tapered beams is accurately assessed by the proposed approach. Additionally, the effects of material distribution, boundary conditions, and tapering parameter on the deflection behavior are presented. Results show that an increase in the power law index increases the flexibility of the functionally graded tapered beams, resulting in higher deflection. Furthermore, lower tapering parameters also result in higher deflection. Compared to other boundary conditions, clamped-clamped boundary conditions demonstrate the best performance in terms of maximum deflection.

Keywords:
functionally graded material; incremental approach; tapered beam; finite element method; Euler Bernoulli beam theory; Timoshenko beam theory

1   Introduction

Functionally graded materials (FGMs) have been of great importance to many researchers for a long time, owing to their wide range of applications in structural mechanics. These newly created materials have promising applications in various fields, such as aerospace, aeronautics, power plants, nuclear, and civil engineering.

A review of the research studies related to the research topic is presented to define a research gap. To solve this problem, the behavior of Timoshenko beam was investigated by Chockalingam et al. [1] using finite element model (FEM). Additionally, for interpolating nodes, the exact shape functions were developed using analytical solutions. An efficient beam formulation for static and vibration analysis of 2D non-prismatic beams with the kinematic assumptions of the Timoshenko beam theory was presented by Vo et al [2] through isogeometric analysis (IGA). The analytic and numerical behaviour of the deformation of non-prismatic beams resting on elastic foundations was investigated by El-Shabrawy et al. [3] using the perturbation method (PM), analytic method, differential quadrature method (DQM), and numerical methods to determine the buckling load and natural frequency with different end supports. The recovery of transverse normal stresses of varying arbitrary cross-section beams was improved by Vilar et al. [4], although it was restricted to homogeneous isotropic materials and also considered the contributions of internal force derivatives.

Recently, a new transverse direct stress distribution in non-prismatic beams using the Hellinger-Reissner principle was examined by Mercuri et al. [5], and an effective strategy was suggested to overcome the coarse predictions of the structural element strength. An effective recovery procedure based on the Jourawski approach by superposing through-the-depth-defined functions that satisfy the traction-free boundary conditions was proposed by Balduzzi et al. [6]. In his previous work, a Timoshenko model for nonprismatic beams capable of computing stresses and deformations for small to moderately tapered beams was derived by Balduzzi et al. [7]. A static bending deformation for the static response of tapered axially functionally graded beams was derived by Nguyen et al. [8]. Several higher-order refined theories for the linear static analysis of functionally graded (FG) beams using a unified formulation was proposed by Giunta et al. [9]. An exact shape function and stiffness matrices of non-prismatic beam elements for the Euler-Bernoulli and Timoshenko beams using a finite-element solution was developed by Shooshtari and Khajavi [10]. The stiffness matrix of the nonprismatic beam was formulated by separating the rigid body motions from the strain modes and determining the strain field. The exact stiffness matrix and shape functions for the homogeneous tapered clamped beam are derived by Franciosi and Mecca [11]. A stiffness matrix for beams with variable cross-sections considering the flexibility approach and the variation in height and width was derived by Eisenberger [12]. Furthermore, the explicit terms for stiffness matrices was obtained by Eisenberger [13] using the flexibility method and considering the effect of transverse shear. An analytical derivation of a symmetric cantilevered linearly tapered Timoshenko beam under transverse and coupled loadings was presented by Wong et al. [14]. The static deflection of a non-prismatic axially functionally graded beam subjected to a distributed load was examined by Hashim et al. [15] using ANSYS Workbench (17.2). Three types of supports were employed by the authors: (1) free-clamped, (2) clamped-free, and (3) simply supported. The elastic modulus of the beam varies continuously in the axial direction of the beam, according to a power-law model. sandwich beams incorporating Functionally Graded Materials (FGM) were investigated by Rezaiee-Pajand et al. [16]; moreover, the investigation was done using two methods: (1) the Ritz method and the principle of minimum total potential energy based on the Timoshenko and Reddy beam theories to evaluate the bending of beams with varying cross sections and a four-node isoparametric beam element was developed by them to analyse porous beams through FGM in [17].

According to the conducted literature review, the majority of previous studies have either considered homogeneous beam properties or axially functionally graded beams or have adopted an analytical approach for FG tapered beams, and there is no antecedent study on the static analysis of these types of structures using transversal gradation of material

properties. This study aims to develop a simple incremental approach based on the finite element method for static analysis of an FG tapered beam. The shape functions and stiffness matrix of FG tapered beams are provided in detail, as they have never been reported before. Nondimensional deflections are examined and presented in detail based on the Euler–Bernoulli and Timoshenko beam theories. The variation in material properties is along the beam thickness and is assumed to follow a power law of the volume fraction of the constituents. Finite element numerical results are presented in both the tabular and graphical forms to determine the effects of the power-law index, tapering parameter, and arbitrary boundary conditions on the static behavior of FG tapered beams.

The presented results will contribute significantly by providing a valuable reference point for future research on tapered FG beams.

2   Material properties of FGM beam

Material properties of FGM beam vary continuously and non-uniformly in the z direction which are derived by Reddy [18]:

$$V_c = \left(\frac{z}{h} + \frac{1}{2}\right)^k \tag{1-a}$$

$$V_m = 1 - V_c \tag{1-b}$$

Where k is the power law index, the non-negative parameter which dictates the variation in material properties through the beam thickness. For k=0, the volume fraction of ceramic becomes 1, and a homogeneous beam consisting only of ceramic is obtained; when the value of   is increases, the metal content in the FGM increases.

It is assumed that the effective material properties of the FGM structure, including Young's modulus E_{eff}, mass density ρ_{eff}, and shear modulus G_{eff}, vary continuously through the beam thickness according to the power-law form, which can be described by:

$$MP_{eff} = MP_m V_m(z) + MP_c V_c(z) \tag{2}$$

Where, MP_m and MP_c stand for material properties of metals and ceramics, respectively.

3   Finite element formulation

3.1   Euler-Bernoulli beam theory (EBT)

The Euler–Bernoulli beam theory is derived from the following assumptions:

o   The cross-section can be assumed as a rigid surface during deformation and can only rotate.
o   The cross-section rotates around a neutral surface that remains in-plane.
o   During deformation, the cross section remains perpendicular to the neutral surface.

3.1.1   Displacement field

According to the first hypothesis, the axial and vertical displacements of any point of an FGM beam section depend only on the axial coordinate x. They are expressed as:

$$u(x,z) = u_0(x) - z\frac{\partial w_0}{\partial x} \tag{3-a}$$

$$w(x,z) = w_0(x) \tag{3-b}$$

Where $u_0(x)$ and $w_0(x)$ are the axial and transverse displacements in the reference plane in the x- and z-directions, respectively. Eqs. (3-a) and (3-b) can be rewritten in the matrix form as follows:

$$\begin{Bmatrix} u \\ w \end{Bmatrix} = \begin{bmatrix} 1 & 0 & -z \\ 0 & 1 & 0 \end{bmatrix} \begin{Bmatrix} u_0 \\ w_0 \\ \dfrac{\partial w_0}{\partial x} \end{Bmatrix} \tag{4}$$

3.1.2 Strains

Assuming small deformations, the displacement-strain relation can be represented by:

$$\varepsilon_{xx} = \frac{\partial u}{\partial x} = \varepsilon_{xx}^0 + z\kappa_{xx}$$

$$\varepsilon_{xx}^0 = \frac{\partial u_0}{\partial x}, \kappa_{xx} = -\frac{\partial^2 w_0}{\partial x^2} \tag{5-a}$$

or:

$$\varepsilon_{xx} = \begin{bmatrix} 1 & -z \end{bmatrix} \begin{Bmatrix} \dfrac{\partial u_0}{\partial x} \\ \dfrac{\partial^2 w_0}{\partial x^2} \end{Bmatrix} \tag{5-b}$$

Where $\varepsilon^0{}_{xx}$ and κ_{xx} are the extensional strain and the bending strain, respectively.

3.1.3 Strains stresses and stress resultants

According to the Hooke's law, the axial stress is defined as:

$$\sigma_{xx} = E(z)\varepsilon_{xx} = E(z) \begin{bmatrix} 1 & -z \end{bmatrix} \begin{Bmatrix} \dfrac{\partial u_0}{\partial x} \\ \dfrac{\partial^2 w_0}{\partial x^2} \end{Bmatrix} \tag{6}$$

Where $E(z)$ is the variation in Young's modulus in the direction of thickness (z).
Based on the minimum potential energy principle, if a body is in equilibrium, the total virtual strain energy caused by the internal forces and virtual potential of the external loads is zero.

$$\delta\pi = \delta(U_I + W_E) = 0 \tag{7}$$

Where δU_I and δW_E are given as:

$$\delta U_I = \int_V \sigma_{xx}\, \delta\varepsilon_{xx} dV = \int_0^L (N\delta\varepsilon_{xx}^0 + M\delta\kappa_{xx}^0)\, dx \tag{8}$$

$$\delta W_E = \int_0^L (q\delta w_0 + f\delta u_0)\, dx \tag{9}$$

N is the normal force and M is the bending moment across the FGM beam section, defined as:

$$N = \int_A \sigma_{xx}\, dA = \widehat{D}_a \varepsilon_{xx}^0 + \widehat{D}_{ab}\kappa_x \tag{10}$$

$$M = \int_A z\sigma_{xx}\, dA = \widehat{D}_{ab}\varepsilon_{xx}^0 + \widehat{D}_b\kappa_x \tag{11}$$

Where $\widehat{D}_a$, $\widehat{D}_b$, are $\widehat{D}_{ab}$ the axial stiffness, bending stiffness, and coupling axial-bending stiffness. These stiffness coefficients can be calculated as:

$$[\widehat{D}_a \quad \widehat{D}_b \quad \widehat{D}_{ab}] = b \int_{-h/2}^{+h/2} E(z)\, [1 \quad z^2 \quad z] dz \tag{12}$$

Where f and q are the distributed forces in the x and z directions, respectively. The variational statement of the FGM Euler-Bernoulli beam can be obtained by substituting Eqs. (10) and (11) into Eqs. (8) and (9) and therefore, into Eq. (7).

$$\int_0^L \begin{bmatrix} \left\{-b\int_{-h/2}^{+h/2} E(z)dz\right\}\dfrac{\partial u_0}{\partial x}\dfrac{\partial \delta u_0}{\partial x} + \left\{b\int_{-h/2}^{+h/2} zE(z)dz\right\}\dfrac{\partial^2 w_0}{\partial x^2}\dfrac{\partial \delta u_0}{\partial x} + \\ \left\{b\int_{-h/2}^{+h/2} zE(z)dz\right\}\dfrac{\partial u_0}{\partial x}\dfrac{\partial^2 \delta w_0}{\partial x^2} - \left\{b\int_{-h/2}^{+h/2} z^2E(z)dz\right\}\dfrac{\partial^2 w_0}{\partial x^2}\dfrac{\partial^2 \delta w_0}{\partial x^2} \\ +f\delta u_0 + q\delta w_0 \end{bmatrix} dx = 0 \qquad (13)$$

3.1.4 Finite element modelling

Nodal displacements and shape functions can be used to write the displacement components. As shown below, they can be expressed as a result of the in-plane and transverse deflection components.

- o In-plane components:

$$U(x) = [N(x)]_u \{q\{t\}\}_u \qquad (14)$$

- o Transverse deflection components:

$$W(x) = [N(x)]_w \{q\{t\}\}_w \qquad (15)$$

Where $[N(x)]$ and $q\{t\}$ represent the shape functions and nodal displacements, respectively (Appendix A); and $[K]$ represents the global stiffness matrix of the FG tapered beam defined in Appendix A.

3.2 Timoshenko beam theory (TBT)

3.2.1 Displacement field

Based on Timoshenko beam theory, the axial and vertical displacements of any point of the beam section can be expressed as:

$$u(x,z) = u_0(x) - z\theta_z(x) \qquad (16)$$

$$w(x,z) = w_0(x) \qquad (17)$$

Where $u_0(x)$ and $w_0(x)$ are the axial and transverse displacements of any point on the mid-plane, respectively, and ϑ_z is the bending rotation. Eqs. (16) and (17) can be rewritten as:

$$\begin{Bmatrix} u \\ w \end{Bmatrix} = \begin{bmatrix} 1 & 0 & -z \\ 0 & 1 & 0 \end{bmatrix} \begin{Bmatrix} u_0 \\ w_0 \\ \theta_z \end{Bmatrix} \qquad (18)$$

3.2.2 Strains

The nonzero strains can be represented by:

$$\varepsilon_{xx} = \frac{\partial u}{\partial x} = \frac{\partial u_0}{\partial x} - z\frac{\partial \theta_z}{\partial x}, \gamma_{xz} = \frac{\partial u}{\partial z} + \frac{\partial w}{\partial x} = -\theta_z + \frac{\partial w_0}{\partial x} \qquad (19\text{-a})$$

Or:

$$\varepsilon = \begin{Bmatrix} \varepsilon_{xx} \\ \gamma_{xz} \end{Bmatrix} = \begin{bmatrix} 1 & -z & 0 \\ 0 & 0 & 1 \end{bmatrix} \begin{bmatrix} \dfrac{\partial u_0}{\partial x} & \dfrac{\partial \theta_z}{\partial x} & \dfrac{\partial w_0}{\partial x} - \theta_z \end{bmatrix}^T \qquad (19\text{-b})$$

3.2.3 Stresses and stress resultants

The constitutive relation for FGM is assumed to be of the form:

$$\sigma_{xx} = E(z)\varepsilon_{xx} = E(z)\left(\frac{\partial u_0}{\partial x} - z\frac{\partial \theta_z}{\partial x}\right) \tag{20}$$

$$\tau_{xz} = G(z)\gamma_{xz} = G(z)\left(-\theta_z + \frac{\partial w_0}{\partial x}\right) \tag{21}$$

It can be expressed in the matrix form as follows:

$$\sigma = \begin{Bmatrix}\sigma_{xx}\\\tau_{xz}\end{Bmatrix} = \begin{bmatrix}E(z) & 0\\0 & G(z)\end{bmatrix}\begin{Bmatrix}\varepsilon_{xx}\\\gamma_{xz}\end{Bmatrix} \tag{22-a}$$

$$\sigma = \begin{Bmatrix}\sigma_{xx}\\\tau_{xz}\end{Bmatrix} = \begin{bmatrix}E(z) & 0\\0 & G(z)\end{bmatrix}\begin{bmatrix}1 & -z & 0\\0 & 0 & 1\end{bmatrix}\begin{bmatrix}\frac{\partial u_0}{\partial x} & \frac{\partial \theta_z}{\partial x} & \frac{\partial w_0}{\partial x} - \theta_z\end{bmatrix}^T \tag{22-b}$$

According to the same procedure applied to the Euler-Bernoulli beams, the normal force, shear force, and bending moment of the Timoshenko FGM beam can be obtained as follows:

$$N = \int_A \sigma_{xx}\, dA = \widehat{D}_a \varepsilon_{xx}^0 + \widehat{D}_{ab}\kappa_x \tag{23}$$

$$Q = \int_A \kappa_s \sigma_{xz} dA = \kappa_s \widehat{D}_s\left(\frac{\partial w}{\partial x} - \theta_z\right) \tag{24}$$

$$M = \int_A z\sigma_{xx}\, dA = \widehat{D}_{ab}\varepsilon_{xx}^0 + \widehat{D}_b\kappa_x \tag{25}$$

Where $[\widehat{D}_s] = b\int_{-h/2}^{+h/2} G(z)\, dz$ for an isotropic beam, the terms containing $\widehat{D}_{ab}$ are equal to zero because of the absence of membrane bending coupling. The variational form of the equilibrium equations of the FGM Timoshenko beam in terms of displacement can be obtained by substituting Eqs. (23), (24) and (25) into Eq. (7).

$$\int_0^L\begin{bmatrix}\left\{-b\int_{-h/2}^{+h/2}E(z)dz\right\}\frac{\partial u_0}{\partial x}\frac{\partial \delta u_0}{\partial x} - \left\{b\int_{-h/2}^{+h/2}zE(z)dz\right\}\frac{\partial \theta_z}{\partial x}\frac{\partial \delta u_0}{\partial x} - \\ \left\{b\int_{-h/2}^{+h/2}zE(z)dz\right\}\frac{\partial u_0}{\partial x}\frac{\partial \delta\theta_z}{\partial x} + \left\{b\int_{-h/2}^{+h/2}z^2E(z)dz\right\}\frac{\partial \theta_z}{\partial x}\frac{\partial \delta\theta_z}{\partial x} \\ + \left\{b\int_{-h/2}^{+h/2}G(z)dz\right\}\left(-\theta_z + \frac{\partial w_0}{\partial x}\right)\left(-\delta\theta_z + \frac{\partial \delta w_0}{\partial x}\right) + f\delta u_0 + q\delta w_0\end{bmatrix}dx = 0 \tag{26}$$

3.2.4 Finite element modelling

The displacement components can be given using shape functions and nodal displacements. They can be expressed as a result of the in-plane, transverse deflection, and shear components, as shown below:

o   In-plane components:

$$U(x) = [N(x)]_u\{q\{t\}\}_u \tag{27}$$

o   Transverse deflection components:

$$W(x) = [N(x)]_w\{q\{t\}\}_w \tag{28}$$

o Shear components:

$$\theta_z(x) = [N(x)]_{\theta_z}\{q\{t\}\}_{\theta_z} \tag{29}$$

Where $[N(x)]$ and $q\{t\}$ represent the shape functions and nodal displacements, respectively (Appendix B), while $[K]$ represents the global stiffness matrix of the FG tapered beam defined in Appendix B.

3.3 Position of the neutral axis

The location of the neutral axis must be determined to proceed. Because of the variation in Young's modulus through the thickness of the FGM beam, the neutral axis is no longer at the mid-plane, but it shifts from the mid-plane, unless for the case of an isotropic beam. Two different planes, z and z_1, were considered, as shown in Figure 1 and Eq. (30):

$$x = x_1, z = z_1 + h_0 \tag{30}$$

Where h_0 is the distance between the neutral axis and mid-plane of the beam.
Following the same procedure as the Euler–Bernoulli beam theory, the strain ε_x and stress σ_x can be obtained as follows:

$$\varepsilon_x = -z_1 \frac{\partial^2 w_0}{\partial x^2} \tag{31}$$

$$\sigma_x = -z_1 E(z_1) \frac{\partial^2 w_0}{\partial x^2} \tag{32}$$

Neutral surfaces can be positioned such that the total axial force at cross section vanishes:

$$\sum F_x = 0 \rightarrow \int_{-h/2+h_0}^{+h/2+h_0} \sigma_x \, dA \tag{33}$$

Substituting Eq. (31) and (32) into Eq. (33), and changing the limits of integration yields:

$$b \int_{-h/2}^{+h/2} E(z) \times (z - h_0) \frac{\partial^2 w_0}{\partial x^2} dz = 0 \tag{34}$$

$$b \frac{\partial^2 w_0}{\partial x^2} \left(\int_{-h/2}^{+h/2} E(z)z dz - h_0 \int_{-h/2}^{+h/2} E(z) dz \right) = 0 \tag{35}$$

The location of the neutral axis is defined as:

$$h_0 = \frac{\widehat{D}_{ab}}{\widehat{D}_a} = \frac{\int_{-h/2}^{+h/2} E(z)z dz}{\int_{-h/2}^{+h/2} E(z) dz} = \frac{nh(E_c - E_m)}{2(n+2)(E_c + nE_m)} \tag{36}$$
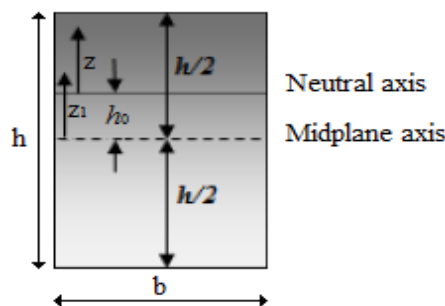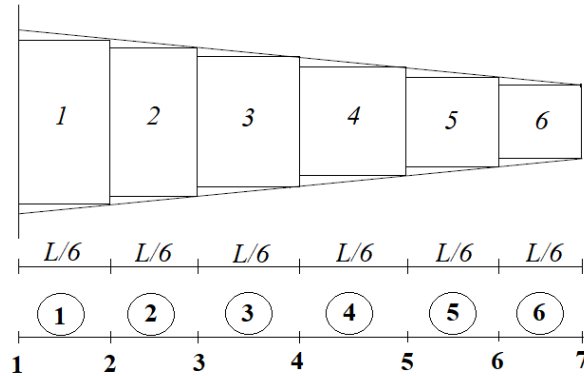

Figure 1. Position of the neutral surface

3.4 Incremental approach for tapered beam

The proposed approach is based on the division of the non-uniform beam into segments of uniform cross-section, where the shape functions and the stiffness matrix derived for the uniform beam can be applied to each segment. Consider a tapered beam subdivided into uniform segments, as shown in Figure 2.

Figure 2. Subdivision of the tapered beam into uniform segments

By adopting a linear equation and using the data at the boundary conditions, the cross-section and moment of inertia at each node can be obtained using the following equations:

$$A(x) = ax + b \tag{37-a}$$

$$h(x) = ax + b = h_0\left(1 + \alpha\frac{x}{L}\right) \tag{37-b}$$

Where α is the tapering parameter:

$$\alpha = \frac{h_0 - h_L}{h_L} \tag{37-c}$$

The moment of inertia can be expressed in terms of as:

$$h(x) = ax + b = h_0\left(1 + \alpha\frac{x}{L}\right) \tag{38-a}$$

$$I(x) = \frac{bh_0^3}{12}\left(1 + \alpha\frac{x}{L}\right)^3 \tag{38-b}$$

Each segment has two nodes, and each of these nodes has their locations; thus, the cross-sectional area and moment of inertia of the uniform beam segment are determined from the average cross-section and average moment of inertia of the corresponding nodes of the beam segment, respectively.

$$A(element\ n) = \frac{(A_n + A_{n+1})}{2} \tag{39-a}$$

$$I(element\ n) = \frac{(I_n + I_{n+1})}{2} \tag{39-b}$$

4   Numerical results and discussions

4.1   Model validation

In this section, various numerical examples are presented and discussed to demonstrate the efficiency of the proposed model in predicting the bending responses of isotropic tapered beams under different loads. Additionally, different boundary conditions (BCs) are considered.

4.1.1 Cantilever tapered beam with point load at free end

In the first example, a cantilever tapered beam subjected to a tip load was analysed to predict the distribution of the reaction forces and the maximum deflection at the free end of the beam (Figure 3. a).
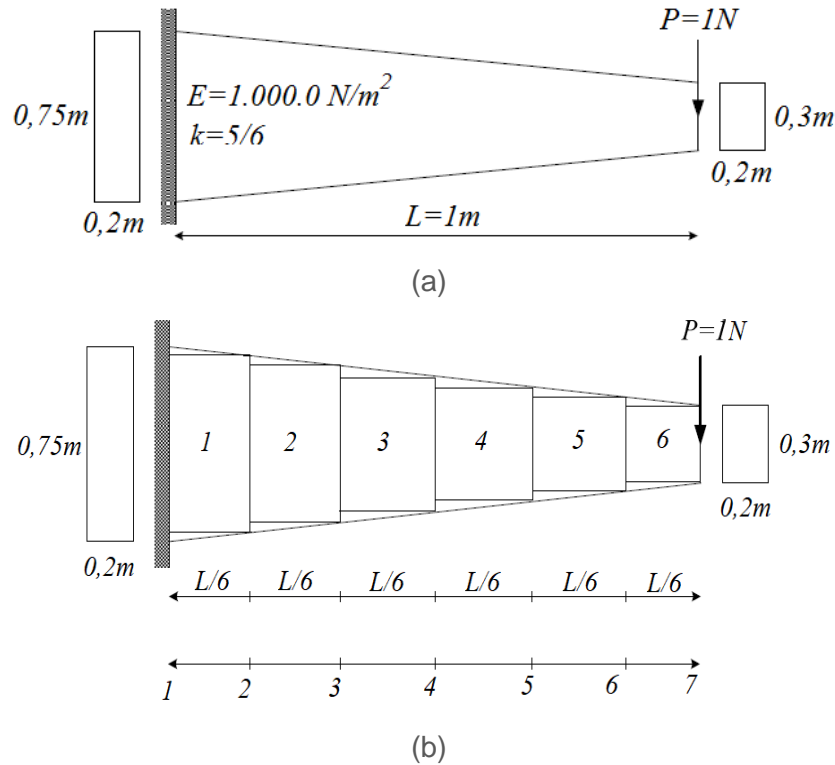

(a)

(b)

Figure 3. (a) Cantilever beam with point load at free end; (b) subdivision of the tapered beam into six uniform elements

The beam was discretised into six elements, as shown in (Figure 3. b) with the shape functions derived in Section 3 for both the beam theories. For validation, the maximum deflection, normal force, and bending moment for a homogenous tapered beam were compared, and the results are listed in Table 1. EBT denotes the results obtained using the Euler-Bernoulli beam theory, where shear deformation is not considered. TBT denotes the results obtained using the Timoshenko beam theory where shear deformation is considered.

It can be observed from the Table that the results obtained by the present method are in good agreement with those obtained by Eisenberger [12] using analytical solutions. The percent differences between the predicted and analytical values of the maximum deflection fall within a range of 0,49 % and 1,78 % for the TBT and EBT, respectively.
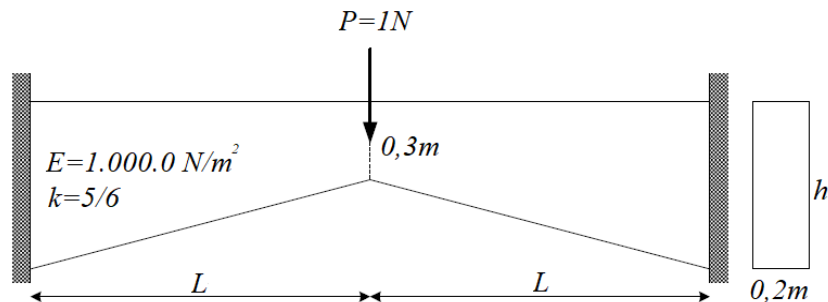
Table 1. Force reactions and maximum deflection at the tip end of the C-F tapered beam

Theories	Q (N)	M (Nm)	Present (10^{-2}m)	Eisenberger [12] (10^{-2}m)	Diff. (%)
EBT	1,0	1,0	0,904	0,897	0,7803
TBT	1,0	1,0	1,197	1,203	0,4987

4.1.2 Clamped-clamped tapered beam with concentrated load

In the second example, the effect of shear deformation was further explored. To achieve this, clamped-clamped (C-C) tapered beams with various heights were used (Figure 4). Twelve

elements were used to discretise the beam. The geometrical and material properties of the tapered beam used in this example are based on Eisenberger [13].

Figure 4. Clamped-clamped beam with height variation

The reaction forces and maximum deflections, including shear deformation using "TBT" and neglecting shear deformation using "EBT" at the middle of the beam, and the percent difference between the two formulations are tabulated in Tables 2 and 3, respectively. It can be observed that the numerical results obtained using the present method are in good agreement with those obtained by Eisenberger [13] for both beam theories using different values of length and height.

Table 2. Reaction forces and maximum deflections of C-C tapered beam (h=0,6 m)

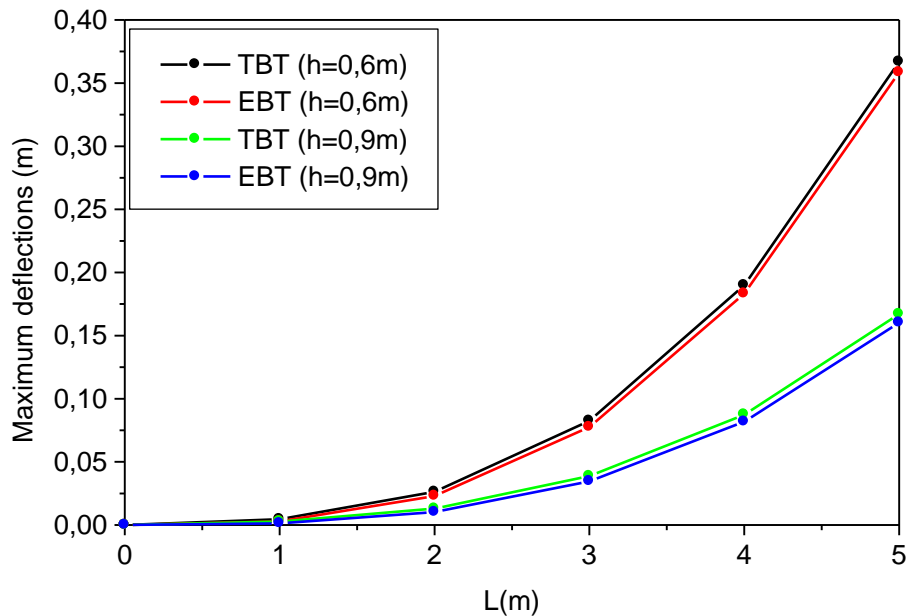| L (m)	Q (N)	M (Nm)	TBT (10^{-2}m)		Diff. (%)	EBT (10^{-2}m)		Diff. (%)
			Present	Eisenberger [13]		Present	Eisenberger [13]	
1	0,5	0,25	0,455	0,468	2,7778	0,288	0,294	2,0408
2	0,5	0,50	2,622	2,700	2,8889	2,290	2,354	2,7188
3	0,5	0,75	8,251	8,464	2,5165	7,752	7,944	2,4169
4	0,5	1,00	18,986	19,524	2,7556	18,322	18,831	2,7030
5	0,5	1,25	36,680	36,645	0,0955	35,850	35,779	0,1984

The percentage differences between the predicted and analytical values of the maximum deflection for the 1st case fall within a range of 0,09-2,88 %. However, for the second case, these differences are in the range 0,61-6,66 %. However, the overall difference is less than 7 %.

Table 3. Reaction forces and maximum deflections of C-C tapered beam (h=0,9 m)

L (m)	Q (N)	M (Nm)	TBT (10^{-2}m)		Diff. (%)	EBT (10^{-2}m)		Diff. (%)
			Present	Eisenberger [13]		Present	Eisenberger [13]	
1	0,5	0,25	0,266	0,274	2,9197	0,129	0,137	5,8394
2	0,5	0,50	1,296	1,370	5,4015	1,023	1,096	6,6606
3	0,5	0,75	3,874	4,110	5,7421	3,464	3,698	6,3277
4	0,5	1,00	8,733	9,315	6,2480	8,187	8,766	6,6051
5	0,5	1,25	16,703	16,807	0,6188	16,019	16,120	0,6266

The effect of L on the maximum deflections at the middle of the tapered beam owing to the concentrated load is presented in Figure 5. The results for both the beam theories were plotted. As expected, the deflections increased with an increase in the beam length. Furthermore, the difference between the values collected by the EBT and TBT theories is more pronounced at small values of length which confirms the importance of using the TBT theory for non-slender

beams. This emphasises the effect of transverse shear, which increases the flexibility of thick beams and therefore increases the deflections.
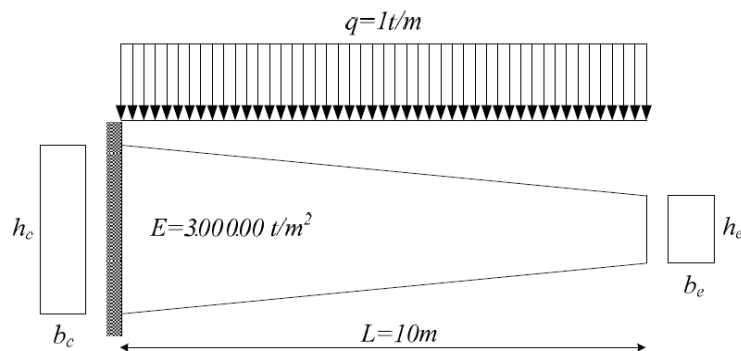

Figure 5. Effect of length L on the maximum deflections at the middle of the tapered beam (C-C)

4.1.3   Cantilever tapered beam with uniformly distributed load

The third example refers to another cantilever tapered Euler-Bernoulli beam with a length of 10 m, subjected to a uniformly distributed load q=1 t/m, Figure 6.
The maximum transverse displacements at the tip are listed in Table 4. The first line "Case A" refers to a beam with unit depth and linearly varying width from 2 m at the clamped end to 0,25 m at the free end. The second line "Case B" refers to a beam with unit width and varying depth between 2 m at the clamped end and 0,25 m at the free end.

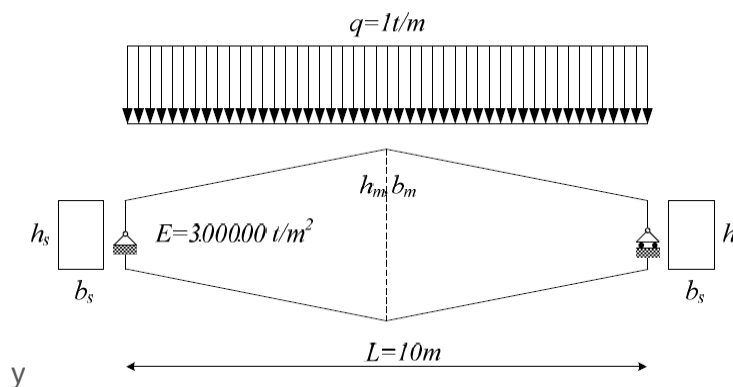**Figure 6. Clamped-free beam subjected to distributed load**

For the material properties of the two cases, the Young's modulus and Poisson's ratio were taken as E=3000,00 t/m^2 and 0,2; respectively (Franciosi and Mecca [11]). The current results were compared with those obtained using the classical approach with 400 cubic Hermitian elements (Franciosi and Mecca [11]). An important agreement was reached between the results obtained using the classical approach and the results presented in terms of the maximum displacement, and a high level of accuracy was observed (a percent error of 1,07 % for case A and 0,79 % for case B).

Table 4. Maximum transverse displacements (10^{-2}m) of cantilever tapered beam at the tip end

Cases	TBT		Diff. (%)	EBT		Diff. (%)
	Present	Franciosi and Mecca [11]		Present	Franciosi and Mecca [11]	
Case A	3,230	/	/	3,191	3,1572	1,0706
Case B	1,570	/	/	1,531	1,5432	0,7906

4.1.4   Simply-supported beam with distributed load

In the fourth example (Figure 7), a simply supported (S-S) tapered beam subjected to a uniformly distributed load was considered.

Figure 7. Simply-supported tapered beam subjected to uniformly distributed load

The maximum transverse displacements at the midspan of the beam are listed in Table 5. The first line "Case A" refers to a beam with unit depth and linearly varying width from 2 m at the clamped end to 0,25 m at the free end. The second line "Case B" refers to a beam with unit width and varying depth between 2 m at the clamped end and 0,25 m at the free end. For the material properties of the two cases, the Young's modulus and Poisson's ratio were taken as E=3000,00 t/m^2 and 0,2; respectively (Franciosi and Mecca [11]). The present results were compared with those obtained using the classical approach with 400 cubic Hermitian elements (Franciosi and Mecca [11]). Good agreement was found with a percent error of 0,88 % for Case A and 3,90 % for Case B.

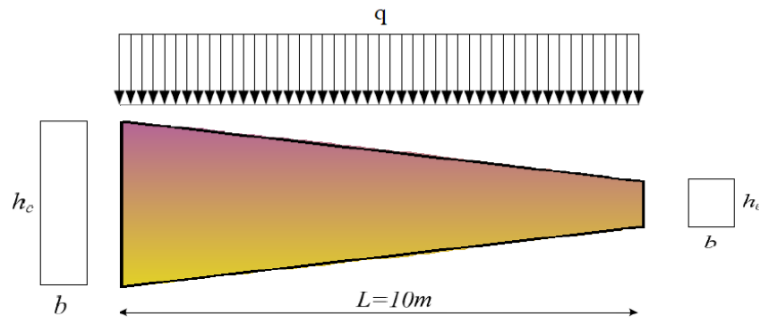**Table 5. Maximum transverse displacements (10^{-2}m) of simply-supported tapered beam at the mid-spam**

Cases	TBT		Diff. (%)	EBT		Diff. (%)
	Present	Franciosi and Mecca [11]		Present	Franciosi and Mecca [11]	
Case A	3,949	/	/	3,768	3,735	0,8835
Case B	2,937	/	/	2,756	2,868	3,9052

Notably, the accuracy of Timoshenko beam theory (TBT) is higher than that of the Euler-Bernoulli beam theory (EBT). The Euler-Bernoulli model tends to slightly underestimate the deflections of non-slender tapered beams. In the design of a tapered beam with a non-slender ratio, the transverse shear should be considered to better predict the deflections.

4.2 Parametric results

After the validation of the isotropic tapered beam, the finite element method was extended to study the static analysis behaviour of the FG tapered beam for various tapering parameters, power law indices, and various end boundary conditions. In this section, only the Timoshenko theory beam was used.

The FG tapered beam is assumed to be composed of ceramic and metal, the material properties of ceramic are E_c= 380 GPa and v_c= 0,2; and those of metal are E_m= 70 GPa and v_m= 0,2; respectively, and subjected to uniformly distributed load as shown in Figure 8. Different boundary conditions are considered.

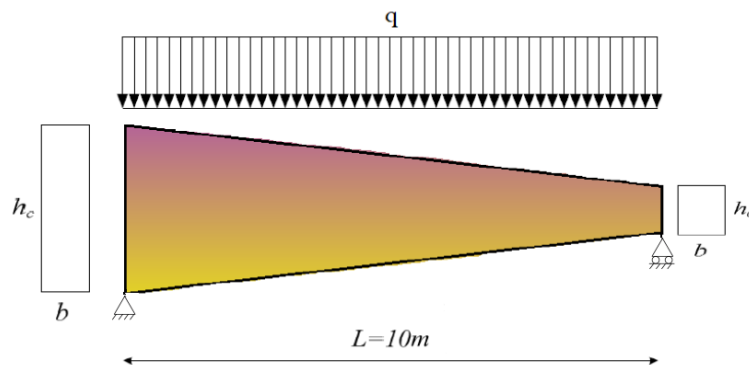**Figure 8. FG tapered beam subjected to uniformly distributed load**

The dimensionless of max deflection is defined as:

$$w^* = w(\text{max}) \frac{5qL^4}{384E_m I_0} \tag{40}$$

Where α=0 refers to a uniform beam (the cross-section is constant along the length): b=0,2 m, h=0,6 m. While α=-0,5 refers to a beam with 0,2 width and linearly varying depth in the range of 0,3-0,6 m (the depth is doubled). The third value α=-0,66 refers to a beam with 0,2 width and varying depth in the range of 0,3-0,9 m (the depth is tripled).

4.2.1 Simply-supported beam (S-S)

A simply supported tapered beam subjected to a uniformly distributed load is illustrated in Figure 9. The effects of the tapering parameter and material distribution profile k on the dimensionless maximum deflection of the S-S beam are presented in Table 6 and Figure 10.
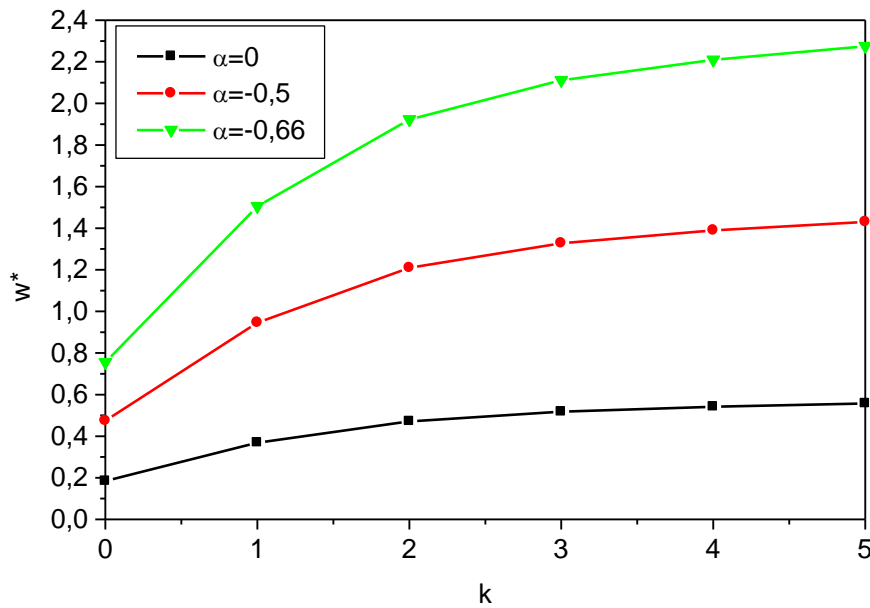

Figure 9. Simply-supported FG tapered beam subjected to uniformly distributed load

As seen from the results, increasing the power law index tends to increase the deflections, and this is due to the fact that an increase in power law index decreases the value of elasticity modulus and hence makes FG tapered beams more flexible. The deflection was proportional to the power-law index. Additionally, it can be observed that as the tapering parameter decreases, the deflections increase. This emphasises the effect of the tapering parameter

which increases the flexibility of the tapered beams and therefore increases the deflection. It is interesting to note also noteworthy that the maximum deflection occurred at the middle of the FG beam.

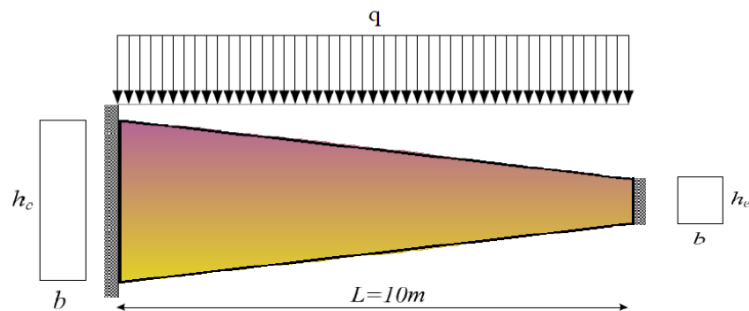**Table 6. Dimensionless of max deflection of S-S FG tapered beams**

k	Non-dimensional deflection w^*		
	$\alpha = 0$	$\alpha = -0,5$	$\alpha = -0,66$
0	0,1844	0,4738	0,7548
1	0,3684	0,9459	1,5049
2	0,4711	1,2091	1,9224
3	0,5175	1,3280	2,1112
4	0,5414	1,3896	2,2094
5	0,5573	1,4305	2,2748

Figure 10. Variation of the dimensionless of max deflection of FG tapered beams (S-S)

4.2.2 Clamped-clamped beam (C-C)

A clamped-clamped tapered beam subjected to a uniformly distributed load is shown in Figure 11. Table 7 and Figure 12 illustrate the effects of the tapering parameter and power-law index on the dimensionless maximum deflection for the C-C tapered beam.
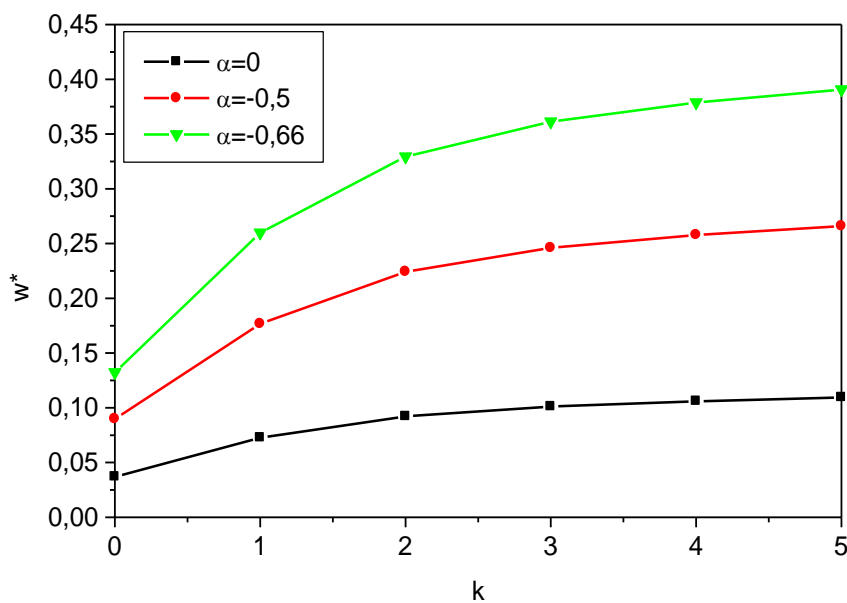

Figure 11. Clamped-clamped FG tapered beam subjected to uniformly distributed load

In light of what was said earlier for the S-S counterparts, increasing the power law index leads to an increase in the deflections for the same tapering parameter. The deflection values

increase as the tapering parameter decreases. Furthermore, compared to the other end conditions, minimum deflections are observed for the C-C beam. Notably, the maximum deflection occurred at the FG tapered beam centre.

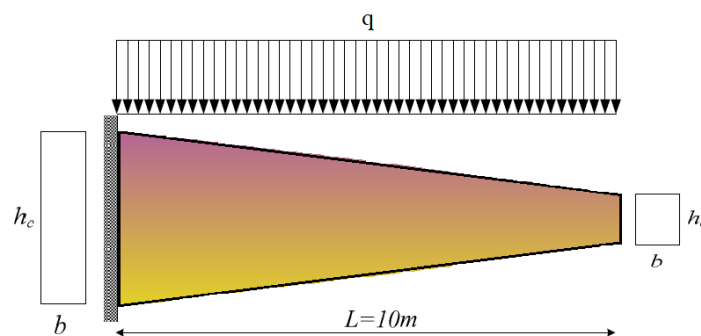**Table 7. Dimensionless of max deflection of C-C FG tapered beams**

k	Non-dimensional deflection w^*		
	$\alpha = 0$	$\alpha = -0,5$	$\alpha = -0,66$
0	0,0369	0,0898	0,1323
1	0,0726	0,1767	0,2598
2	0,0922	0,2242	0,3293
3	0,1012	0,2460	0,3613
4	0,1060	0,2578	0,3787
5	0,1094	0,2659	0,3907

Figure 12. Variation of the dimensionless of max deflection of FG tapered beams (C-C)

4.2.3   Clamped-free beam (C-F)

Figure 13 shows a clamped-free tapered beam subjected to a uniformly distributed load. Table 8 and Figure 14 show the effects of the tapering parameter and power law index on the dimensionless maximum deflection for the C-F tapered beam.
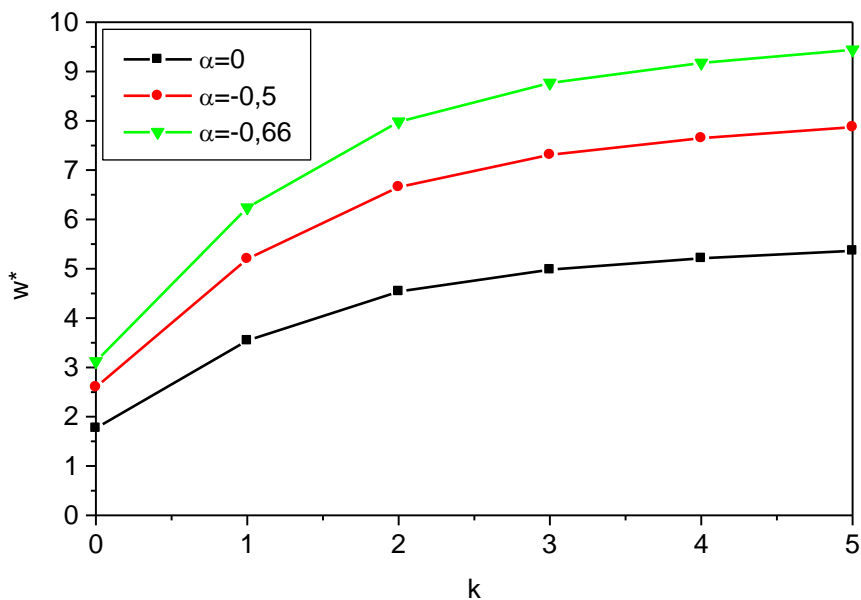

Figure 13. Clamped-free FG tapered beam subjected to uniformly distributed load

A similar observation can be made in Table 7 and Figure 12. The deflections showed an ascending trend when the power-law index increases (Figure 10). The minimum deflection values were obtained for the full ceramic beams (k=0) for all tapering parameters considered (0; -0,5 and -0,66). Compared to the S-S and C-C boundary conditions, the deflections with C-F are more strongly affected by the power law index and tapering parameter. The maximum deflection occurred at the free end of the FG tapered beam.

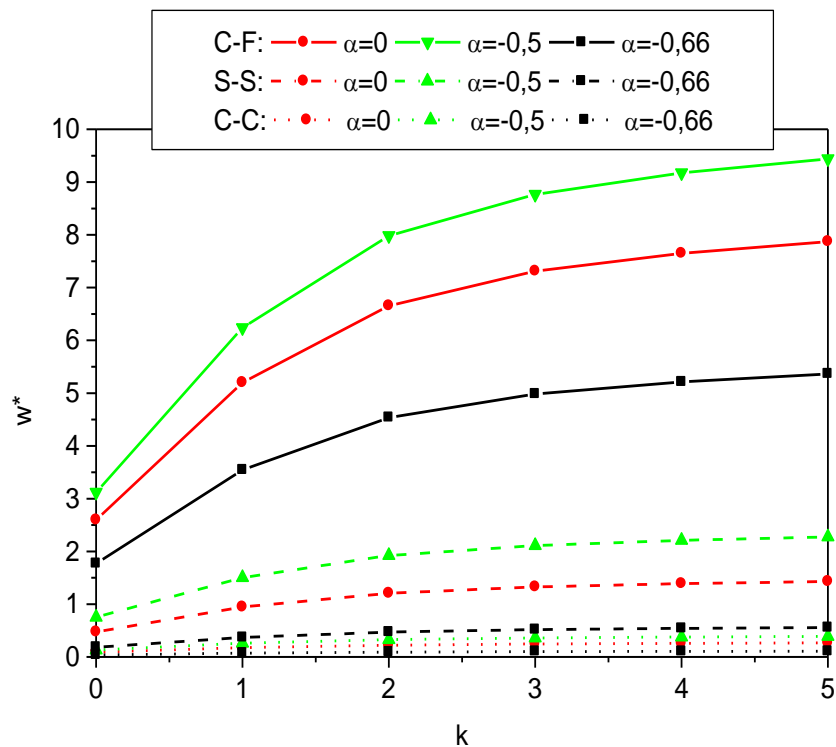**Table 8. Dimensionless of max deflection of C-F FG tapered beams**

k	Non-dimensional deflection w^*		
	$\alpha = 0$	$\alpha = -0,5$	$\alpha = -0,66$
0	1,7698	2,5984	3,1186
1	3,5438	5,2003	6,2382
2	4,5367	6,6555	7,9819
3	4,9834	7,3104	8,7670
4	5,2131	7,6480	9,1727
5	5,3646	7,8709	9,4405

Figure 14. Variation of the dimensionless of max deflection of FG tapered beams (C-F)

Figure 15 shows the effect of the power law index k on the dimensionless maximum deflections for various boundary conditions. As observed from the Figure, increasing the power law index tends to increase the deflections, and this is due to the fact that an increase in power law index results in a decrease in the value of elasticity modulus, thus making FGM beams more flexible. The deflection was proportional to the power-law index. Additionally, for all the boundary conditions considered, the values of the deflection for α=0 were lower than those for the other tapering parameter (-0,5 and -0,66). Additionally, it is worth noting that, for a constant power law index and identical α, the values of the non-dimensional maximum deflection with C-F FGM beam are higher than those for the other boundary conditions (S-S and C-C); this is due to the fact that a change in the boundary conditions reflects a change in the beam's rigidity. In other words, as the rigidity of the structure increased, the deflection decreased.

Figure 15. Variation of the dimensionless of max deflection of FG tapered beams for different boundary conditions

5   Conclusions

In this study, an incremental approach was developed to investigate the static analysis of FG tapered beams. This approach consists of subdividing non-uniform beams into segments with uniform cross-sections. Two separate finite element models were developed, one is used to analyse the structural behavior of slender beams (Euler-Bernoulli theory) and the other is used for deep beams (Timoshenko Beam Theory). The shape functions and stiffness matrix are provided in detail, as they have not been presented elsewhere. The effects of the material distribution, boundary conditions, and tapering parameter on the deflection are presented and determined.

Based on the above study, the following conclusions can be drawn:

- o A comparison with the data from the literature shows that the formulated element can effectively evaluate the response of tapered beams with an overall difference of less than 7 %.
- o For a constant tapering parameter, the deflections tended to increase as the power-law index increased. This is due to the fact that an increase in the power law index decreases the elasticity modulus and therefore makes FG tapered beams more flexible. The deflections are proportional to the power-law index.
- o For a constant power law index and identical tapering parameter, the values of the dimensionless maximum deflection with C-F FG tapered beam are higher than those for the other boundary conditions (S-S and C-C). This is due to the fact that the changes in the boundary conditions result in changes in the beam's stiffness. Hence, as the structural rigidity increased, the deflection decreased.
- o The deflection values increase as the tapering parameter decreases, which highlights the effect of the tapering parameter on enhancing the flexibility of tapered beams, thus augmenting their deflection.

To minimize the deflections in the FG tapered beam, the geometry and material properties can be tailored by selecting a suitable tapering parameter, power law index and boundary conditions.

Appendix A - Euler-Bernoulli beam theory

The shape functions are:

$$N_1(\xi) = \frac{1-\xi}{2} \tag{41-a}$$

$$N_2(\xi) = \frac{1+\xi}{2} \tag{41-b}$$

$$
\begin{aligned}
N_1(\xi) &= \frac{1}{4}(2 - 3\xi + \xi^3) \\
N_2(\xi) &= \frac{1}{4}(1 - \xi - \xi^2 + \xi^3) \\
N_3(\xi) &= \frac{1}{4}(2 + 3\xi - \xi^3) \\
N_4(\xi) &= \frac{1}{4}(-1 - \xi + \xi^2 + \xi^3)
\end{aligned}
\tag{41-c}
$$

The parametric to real element transition is done by:

$$dx = \frac{\partial x}{\partial \xi} d\xi = \frac{L}{2} d\xi \tag{42}$$

The global stiffness matrix for Euler-Bernoulli beam is:

$$
[K] = \begin{bmatrix}
\dfrac{\hat{D}_a}{L} & 0 & \dfrac{-\hat{D}_{ab}}{L} & \dfrac{-\hat{D}_a}{L} & 0 & \dfrac{\hat{D}_{ab}}{L} \\
0 & \dfrac{12\hat{D}_b}{L^3} & \dfrac{6\hat{D}_b}{L^2} & 0 & \dfrac{-12\hat{D}_b}{L^3} & \dfrac{6\hat{D}_b}{L^2} \\
 & & \dfrac{4\hat{D}_b}{L^2} & \dfrac{\hat{D}_{ab}}{L} & \dfrac{-6\hat{D}_b}{L^2} & \dfrac{2\hat{D}_b}{L} \\
 & & & \dfrac{\hat{D}_a}{L} & 0 & \dfrac{-\hat{D}_{ab}}{L} \\
 & & & & \dfrac{12\hat{D}_b}{L^3} & \dfrac{-6\hat{D}_b}{L^2} \\
 & & & & & \dfrac{4\hat{D}_b}{L}
\end{bmatrix}
\tag{43}
$$

Appendix B - Timoshenko beam theory

$$N_1(\xi) = \frac{1-\xi}{2} \tag{44-a}$$

$$N_2(\xi) = \frac{1+\xi}{2} \tag{44-b}$$

$$
\begin{aligned}
N_{1w}(\xi) &= \frac{1}{8(1+\phi_z)}\left(2(\xi-1)(\xi^2+\xi-2-2\phi_z)\right) \\
N_{2w}(\xi) &= \frac{1}{8(1+\phi_z)}\left(L(\xi^2-1)(\xi-1-\phi_z)\right) \\
N_{3w}(\xi) &= \frac{1}{8(1+\phi_z)}\left(-2(\xi+1)(\xi^2-\xi-2-2\phi_z)\right) \\
N_{4w}(\xi) &= \frac{1}{8(1+\phi_z)}\left(L(\xi^2-1)(\xi+1+\phi_z)\right)
\end{aligned}
\tag{44-c}
$$

The parametric to real element transition is done by:

$$dx = \frac{\partial x}{\partial \xi} d\xi = \frac{L}{2} d\xi \tag{45}$$

The global stiffness matrix for Timoshenko beam is:

$$[K] = \begin{bmatrix} \frac{\hat{D}_a}{L} & 0 & \frac{-\hat{D}_{ab}}{L} & \frac{-\hat{D}_a}{L} & 0 & \frac{\hat{D}_{ab}}{L} \\ 0 & \frac{12\hat{D}_b}{L^3(1+\phi_z)} & \frac{6\hat{D}_b}{L^2(1+\phi_z)} & 0 & \frac{-12\hat{D}_b}{L^3(1+\phi_z)} & \frac{6\hat{D}_b}{L^2(1+\phi_z)} \\ & & \frac{\hat{D}_b(4+\phi_z)}{L(1+\phi_z)} & \frac{\hat{D}_{ab}}{L} & \frac{-6\hat{D}_b}{L^2(1+\phi_z)} & \frac{\hat{D}_b(2-\phi_z)}{L(1+\phi_z)} \\ & & & \frac{\hat{D}_a}{L} & 0 & \frac{-\hat{D}_{ab}}{L} \\ & & & & \frac{12\hat{D}_b}{L^3(1+\phi_z)} & \frac{-6\hat{D}_b}{L^2(1+\phi_z)} \\ & & & & & \frac{\hat{D}_b(4+\phi_z)}{L(1+\phi_z)} \end{bmatrix} \tag{46}$$

References

[1] Chockalingam, S. N.; Pandurangan, V.; Nithyadharan, M. Timoshenko beam formulation for in-plane behaviour of tapered monosymmetric I-beams: Analytical solution and exact stiffness matrix. *Thin-Walled Structures*, 2021, 162. https://doi.org/10.1016/j.tws.2021.107604

[2] Vo, D.; Li, X.; Nanakorn, P.; Bui, T. Q. An efficient isogeometric beam formulation for analysis of 2D non-prismatic beams. *European Journal of Mechanics - A/Solids*, 2021, 89. https://doi.org/10.1016/j.euromechsol.2021.104280

[3] ElShabrawy, M.; Abdeen, M. A.; Beshir, S. Analytic and numeric analysis for deformation of non-prismatic beams resting on elastic foundations. *Beni-Suef University Journal of Basic and Applied Sciences*, 2021, 10. https://doi.org/10.1186/s43088-021-00144-5

[4] Vilar, M. M. S.; Hadjiloizi, D. A.; Masjedi, P. K.; Weaver, P. M. Stress analysis of generally asymmetric non-prismatic beams subject to arbitrary loads. *European Journal of Mechanics - A/Solids*, 90. https://doi.org/10.1016/j.euromechsol.2021.104284

[5] Mercuri, V.; Balduzzi, G.; Asprone, D.; Auricchio, F. Structural analysis of non-prismatic beams: Critical issues, accurate stress recovery, and analytical definition of the Finite Element (FE) stiffness matrix. *Engineering Structures*, 213. https://doi.org/10.1016/j.engstruct.2020.110252

[6] Balduzzi, G.; Aminbaghai, M.; Auricchio, F.; Füssl, J. Planar Timoshenko-like model for multilayer non-prismatic beams. *International Journal of Mechanics and Materials in Design*, 2018, 14, pp. 51-70. https://doi.org/10.1007/s10999-016-9360-3

[7] Balduzzi, G. et al. Non-prismatic Beams: A Simple and Effective Timoshenko-like Model. *International Journal of Solids and Structures*, 2016, 90, pp. 236-250. https://doi.org/10.1016/j.ijsolstr.2016.02.017

[8] Nguyen, T. et al. Static analysis of transversely or axially functionally graded tapered beams. *Materials Research Innovations*, 2014, 18 (sup2: CMSE-2013). https://doi.org/10.1179/1432891714Z.000000000419

[9] Giunta, G.; Belouettar, S.; Carrera, E. Analysis of FGM beams by means of a unified formulation. In: *9th World Congress on Computational Mechanics and 4th Asian Pacific Congress on Computational Mechanics*, 19-23 July 2010, Sydney, Australia: IOP Conference Series Materials Science and Engineering. https://doi.org/10.1088/1757-899X/10/1/012073

[10] Shooshtari, A.; Khajavi, R. An efficient procedure to find shape functions and stiffness matrices of nonprismatic Euler–Bernoulli and Timoshenko beam elements. *European Journal of Mechanics - A/Solids*, 2010, 29 (5), pp. 826-836. https://doi.org/10.1016/j.euromechsol.2010.04.003

[11] Franciosi, C.; Mecca M. Some finite elements for the static analysis of beams with varying cross section. *Computers & Structures*, 1998, 69 (2), pp. 191-196. https://doi.org/10.1016/S0045-7949(98)00094-7

[12] Eisenberger, M. Explicit stiffness matrices for non-prismatic members. *Computers & Structures,* 1985, 20 (4), pp. 715-720. https://doi.org/10.1016/0045-7949(85)90032-X

[13] Eisenberger, M. Stiffness matrices for non-prismatic members including transverse shear. *Computers & Structures*, 1991, 40 (4), pp. 831-835. https://doi.org/10.1016/0045-7949(91)90312-A

[14] Wong, F. T. et al. On the Derivation of Exact Solutions of a Tapered Cantilever Timoshenko Beam. Civil Engineering Dimensions, 2019, 21 (2). https://doi.org/10.9744/ced.21.2.89-96

[15] Hashim W. M.; Alansari L. S.; Aljanabi M.; Raheem H. M. Investigating Static Deflection of Non-Prismatic Axially Functionally Graded Beam. *Material Design & Processing Communications*, 2022. https://doi.org/10.1155/2022/7436024

[16] Rezaiee-Pajand, M.; Masoodi, A.R.; Mokhtari, M. Static analysis of functionally graded non-prismatic sandwich beams. *Advances in Computational Design*, 2018, 3 (2), pp. 165-190. https://doi.org/10.12989/acd.2018.3.2.165

[17] Rezaiee-Pajand, M.; Rajabzadeh-Safaei, N.; Masoodi, A. R. An efficient curved beam element for thermo-mechanical nonlinearanalysis of functionally graded porous beams. *Structures*, 2020, 28, pp. 1035-1049. https://doi.org/10.1016/j.istruc.2020.08.038

[18] Reddy J. N. Analysis of functionally graded plates. International Journal for Numerical Methods in Engineering, 2000, 47 (1-3), pp. 663-684. https://doi.org/10.1002/(SICI)1097-0207(20000110/30)47:1/3<663::AID-NME787>3.0.CO;2-8